Comparison of Adaptive P/ω Droop Strategies for Intermittent Energy Sources in Emergency Islanded Operation

Candelaria Utrilla, Vincent Debusschere, Jérôme Buire, Hossein Dehghani Tafti, Josep Pou, Nouredine Hadjsaid

Comparison of Adaptive P/ω Droop Strategies for Intermittent Energy Sources in Emergency Islanded Operation

Candelaria Utrilla[a], Vincent Debusschere[a], Jérôme Buire[a], Hossein Dehghani Tafti[b], Josep Pou[c], Nouredine Hadjsaid[a,d]

[a]*Univ. Grenoble Alpes, CNRS, Grenoble INP*, G2Elab, 38000 Grenoble, France*
[b]*Department of Electrical, Electronic and Computer Engineering, University of Western Australia, Crawley WA 6009, Australia*
[c]*School of Electrical and Electronic Engineering, Nanyang Technological University, Singapore 639798, Singapore*
[d]*Nanyang Technological University, Singapore 639798, Singapore*

Abstract

Islanded operation is a key tool to improve the reliability and operational resilience of distribution grids. To enable islanded operation with minimal hardware changes, it is convenient to operate already installed PV units in droop-controlled grid-forming mode. This paper analyzes the main adaptive strategies that allow to implement the P/ω droop principle in double-stage units interfacing intermittent energy sources. The advantages and unwanted behaviors of each strategy are illustrated through a thorough simulation-based evaluation, which leads to a set of guidelines for the design of novel improved adaptive P/ω droop strategies.

Keywords: droop control, grid-forming, islanded operation, reliability, renewable energy sources, resilience

*Institute of Engineering Univ. Grenoble Alpes

1. Introduction

In the past decades, distribution grids have experienced a massive increase of distributed generators (DGs), which is revolutionizing their traditional operation. For instance, the DGs development brings production closer to consumption, which opens up the possibility of operating certain distribution grid areas in islanded mode.

More precisely, such areas, which can be denoted as "microgrids", could be operated in islanded mode whenever the main grid is not available. This happens either because of an outage in the upstream grid or, in the case of radial schemes, because an element linking the microgrid to the upstream grid (e.g., a line or a substation) becomes unavailable. Extreme weather events (heatwaves, wildfires, cyclones, floods) are often behind such unavailabilities. Furthermore, such events have been very frequent in the past years and are expected to increase because of climate change [1]. For instance, wildfires can cause multiple faults in several parts of a grid and lead to power cuts in certain areas. Moreover, to prevent wildfires from igniting, grid operators are forced to de-energize certain grid sections in periods of high fire hazard, which leads to further outages. This often happens in California, which experienced 70 "public safety power shut-off" events from 2019 to 2021 [2]. Floods, another example of extreme weather event, also force to de-energize grid areas for safety reasons. This was the case, for instance, during the January 2020 floods in the Greater Jakarta area, which forced to turn off around 2500 distribution substations [3].

Such extreme events explain why distribution system operators are increasingly interested in temporary islanded operation [4], as it is a promising tool to mitigate the consequences of climate change and therefore improve the reliability and operational resilience of electrical grids [5]. More precisely, temporary islanded operation is achieved by isolating the areas affected by an outage and using the DGs to feed the local loads. The islanded microgrids powered with DGs could even be used to energize other parts of the upstream distribution and transmission grids, to accelerate service restoration [6].

Among the different kinds of DGs, photovoltaic (PV) plants are very common and even dominant in areas with good irradiation levels [7]. These are inverter-based generators, which usually operate in grid-feeding mode since they are conceived for grid-connected operation. This fact poses a true challenge for islanded operation, as each microgrid requires at least one grid-forming source to regulate the voltage and the frequency, and to mitigate the generation-consumption unbalances. One possible solution is to enable the grid-forming operation of one of the DGs of the microgrid to be islanded, or to install a new DG with this functionality. The main drawback of this approach is that the grid-forming unit needs to have a relatively large power reserve to handle the generation-consumption unbalances on its own. An alternative is a communication-based solution, such as a master-slave system, but it would require a communication infrastructure. This is a considerable disadvantage, because of the investment required to build the channels and because of the potentially reduced reliability of the system in the event of communication failures. To cope with this issue, the most common approach is to turn to a droop control [8, 9]. This is a decentralized solution (i.e., configured with local controls on each DG) that allows the proper allocation of active and reactive power among multiple generating sources (i.e., to perform a primary control). To enable the islanded operation of PV-dominated distribution grids, it is thus propitious to operate already-installed PV plants in droop-controlled grid-forming mode. There is,

however, a major drawback in the traditional P/ω droop: it is based on an invariable function, as it has been designed for generators with an invariable available active power (normally equal to the maximum rated power). Consequently, this droop strategy is not appropriate for inverters interfacing intermittent energy sources such as PV arrays, whose available power depends on the ambient conditions. It is therefore necessary to design adaptive P/ω droop strategies, to ensure a proper active power allocation in islanded microgrids sustained by PV plants.

This issue has already been addressed by certain research works. Some of them propose to modify the P/ω function by adding a term dependent on the inverter dc bus voltage [10, 11, 12]. Other works propose to use an estimation of the available active power [13, 14, 15, 16, 17]. All these adaptive P/ω droop strategies lead to different behaviors of the islanded microgrids but, to the best of the authors' knowledge, there is no previous work proposing a comparative analysis of these strategies. This work aims to fill this gap. More precisely, its main contributions are:

- A detailed analysis of the "frequency signaling" and "proportional power sharing" capabilities associated to traditional droop control. These capabilities are often mentioned in the literature when evaluating droop control or other primary control strategies. However, what is hardly ever explained is the practical impact such capabilities have on microgrid operation and why they are essential to achieve a proper droop-based primary control. To solve this, section 2 gathers a thorough analysis of both capabilities and explains how they can be lost when the traditional P/ω droop is applied to intermittent energy sources.

- A thorough simulation-based analysis and comparison of the main adaptive P/ω droop strategies found in the literature, presented in section 4. As mentioned, to the best of the authors' knowledge, such analysis has never been conducted in the past. Section 3 describes the used simulation model.

- A set of guidelines extracted from the previous analysis and that aims at facilitating the design of novel and improved adaptive P/ω droop strategies. These guidelines are exposed in section 5, together with the concluding remarks of the paper.

It should be noted that this research is focused on double-stage systems. This is a common PV unit topology that facilitates the implementation of the grid-forming functionality: the inverter regulates the ac voltage and frequency, while the dc/dc converter regulates the power delivered by the PV array, to ensure the microgrid consumption-generation balance.

Another important point to highlight is that, besides from the droop paradigm, there are other inverter control techniques that allow to achieve both the grid-forming and decentralized primary control functionalities. These are, for instance, the virtual synchronous machine (VSM) or the virtual oscillator control (VOC). However, the articles found that try to adapt the decentralized primary control functionality to intermittent energy sources are all based on the droop paradigm, probably because it is the most widely used control. Furthermore, [18, 19] highlight the resemblance between droop control and certain other paradigms, in terms of dynamic and steady-state behavior.

On another note, regarding the droop paradigm, it is important to highlight that the traditional P/ω droop function, from which the adaptive droops here analyzed are derived, has well known disadvantages. These disadvantages are however not addressed in this paper as they have already been very much explored in the literature, in which many droop variants are proposed [8, 20]. Moreover, certain of these variants would be compatible with the adaptive droop strategies analyzed in this paper, as they would not alter the P/ω droop profiles (i.e., the P/ω droop steady-state behavior) built by these strategies. For instance, it is possible to implement such strategies in combination with a virtual impedance [21], in order to improve the dynamic behavior of the P/ω droop function when the lines are not predominantly inductive. Additionally, the virtual impedance principle also allows to properly share harmonic power [22], which is not achieved by the traditional P/ω droop.

Note finally that the traditional Q/V droop function, whose formulation is found in [23], is maintained in the simulations here presented. Although this function also has well-known limitations, these are not addressed as this paper is focused on active power control, and because such limitations have already been thoroughly addressed in the literature [8].

2. Traditional P/ω droop control

2.1. Principle

Suppose an islanded microgrid with n inverter-based units (also called "units" hereafter), interfacing a generic dispatchable energy source, and controlled in grid-forming mode and with the traditional P/ω droop control. Fig. 1(a) represents one of these units, together with its control scheme.

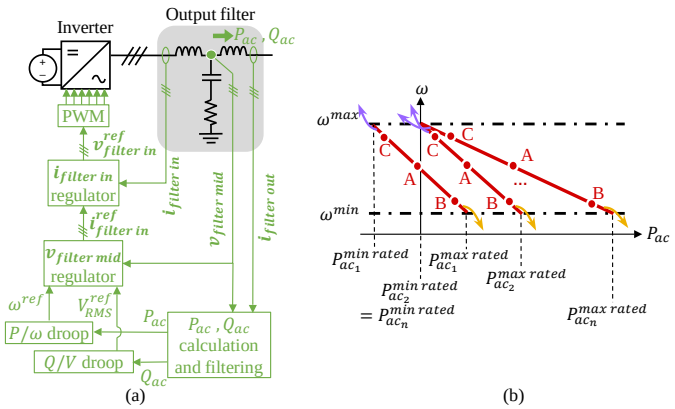

Figure 1: (a) Grid-forming unit with the traditional P/ω droop control. (b) Droop profiles of a microgrid with n units configured with the traditional P/ω droop control.

First, the active power (P_{ac}) and reactive power (Q_{ac}) delivered by the unit are measured and filtered. These are used as inputs for the droop equations, to set the frequency reference (ω^{ref}) and the voltage magnitude reference (V^{ref}_{RMS}) in turn

transmitted to the inner voltage regulator. The traditional P/ω droop is formulated as:

$$\omega^{ref}(t) = \omega^{max} - m_p \left(P_{ac}(t) - P_{ac}^{min\,rated}\right) \quad \text{with } m_p = \frac{\omega^{max} - \omega^{min}}{P_{ac}^{max\,rated} - P_{ac}^{min\,rated}} \quad (1)$$

where $P_{ac}^{max\,rated}$ and $P_{ac}^{min\,rated}$ are the maximum and minimum rated active powers of the unit, m_p is its P/ω droop slope and $(\omega^{max} - \omega^{min})$ delimits the range of allowed frequency values for the islanded microgrid. Equation (1) can also be represented with profiles in the $[P_{ac}, \omega]$ plane, as shown in Fig. 1(b). Note that a droop profile depicts the set of steady state operating points that a unit can reach according to its configured droop strategy.

Following the droop control, there is an outer block that regulates the filter midpoint voltage ($v_{filter\,mid}$), ensuring the grid-forming functionality. The control scheme is completed with an inner control loop that regulates the inverter output current ($i_{filter\,in}$) by setting the output voltage ($v_{filter\,in}^{ref}$).

One of the key characteristics of P/ω droop control is that all the nodes of a synchronous ac grid reach an equal frequency in steady state. This forces the n units of the microgrid to settle at the same frequency, such as in operating point A of Fig. 1(b). If a disturbance such as a load increase occurs, but the total consumed active power in the microgrid (P_{cons}) is smaller than the sum of the units maximum rated active powers (i.e., $P_{cons} < \sum_{i=1}^{n} P_{ac_i}^{max\,rated}$), their droop controls force the microgrid to reach a new steady state such as point B. Conversely, if a load decrease with $P_{cons} > \sum_{i=1}^{n} P_{ac_i}^{min\,rated}$ occurs, the microgrid reaches a new steady state such as point C. Another combined consequence of the global nature of the frequency and of the presented droop formulation is that the frequency of all the microgrid nodes tends jointly to values smaller than ω^{min} only if $P_{cons} > \sum_{i=1}^{n} P_{ac_i}^{max\,rated}$ (see the yellow arrows of Fig. 1(b)). And the frequency of all the microgrid nodes tends jointly to values greater than ω^{max} only if $P_{cons} < \sum_{i=1}^{n} P_{ac_i}^{min\,rated}$ (purple arrows).

It is deduced from the above that the P/ω droop formulation of (1) leads to four different features, explained here below. Two of these features are essential to guarantee a proper functioning of the islanded microgrid, while the other two can be considered as accessory features.

- The presented P/ω droop formulation makes the frequency become a useful indicator of the units loading. This fact, often referred to as "bus signaling" (or more precisely as "frequency signaling") [15], leads to the following two features:

    1. *The frequency limits signal the trespassing of active power limits* (essential). As explained, when $P_{cons} > \sum_{i=1}^{n} P_{ac_i}^{max\,rated}$, every unit trespasses its maximum rated active power (i.e., $P_{ac_i} > P_{ac_i}^{max\,rated}\ \forall i$) and the frequencies of all the nodes jointly decrease under ω^{min}. This value can therefore be used to configure load shedding underfrequency relays (UF relays), to decrease the loading of the units. Conversely, ω^{max} can be also used to configure overfrequency relays (OF relays) that disconnect grid-feeding elements and increase the loading of the grid-forming units.
    2. *Fast reactivity of frequency-based protection mechanisms* (accessory). Fig. 1(b) demonstrates that the frequency of the microgrid progressively diminishes or increases as the loading of the units increases or diminishes. For instance, if all the units are close to their maximum rated active powers, the frequency will stabilize at a value close to ω^{min} (e.g., point B). In this situation, an additional load increase will provoke a fast reduction under ω^{min} and a quick actuation of the UF relay. An analogous behavior is obtained at low loadings regarding the OF relays configured at ω^{max}.

- Additionally, the presented P/ω droop formulation ensures that, in steady state, every unit delivers an active power proportional to its active power range. This fact, commonly known as "proportional power sharing", leads to two features:

    1. *No individual unit loss* (essential). If a unit trespasses its active power limits and no protection measure is taken, it may fail or auto-disconnect in prevention. This is because the active power limits of a unit usually coincide with the power limits of the energy source placed behind it. However, in the presented P/ω droop formulation, no unit converges to an operating point with $P_{ac_i} > P_{ac_i}^{max\,rated}$ if there are other units in the microgrid that have not reached this limit. All the units exceed their maximum rated active powers jointly, and UF protections are activated in this case to impede the loss of units. Conversely, no unit converges to an operating point with $P_{ac_i} < P_{ac_i}^{min\,rated}$ if there are other units in the microgrid that have not reached this limit. All the units go below their minimum rated active powers jointly, and OF protections are activated.
    2. *Reach of active power limits at equal pace* (additional). Fig. 1(b) shows that, at any steady state, the headrooms of all units to increase their active powers are equal, if expressed in proportion to their active power ranges (i.e., $\frac{P_{ac_i}^{max\,rated} - P_{ac_i}}{P_{ac_i}^{max\,rated} - P_{ac_i}^{min\,rated}} = \frac{P_{ac_j}^{max\,rated} - P_{ac_j}}{P_{ac_j}^{max\,rated} - P_{ac_j}^{min\,rated}}$, $\forall\{i, j\}$). Conversely, the headrooms of all units to decrease their active powers are equal. These two facts are important because, as explained above, the headroom of a unit to increase or decrease its active power usually coincides with the headroom of the energy source placed behind it to increase or decrease its power production. Therefore, proportional active power headrooms favor similar internal regulation performances (e.g., the capability to regulate the dc bus voltage v_{dc})

2.2. Limitations

In section 2.1, it is supposed that the inverter-based units interface dispatchable energy sources, where $P_{ac}^{max\,rated}$ always coincides with the available active power (P_{ac}^{avai}). This is however not true for renewable energy sources such as PV arrays, in which P_{ac}^{avai} is conditioned by the intermittency of the energy source. Consequently, the traditional P/ω droop control loses its essential features. This can be easily demonstrated with the example scenario depicted in Fig. 2. Unit 1 is exposed to full irradiation and, therefore, $P_{ac_1}^{avai} = P_{ac_1}^{max\,rated}$. On the contrary, the irradiation received by Unit 2 is lower, reason why $P_{ac_2}^{avai} < P_{ac_2}^{max\,rated}$.

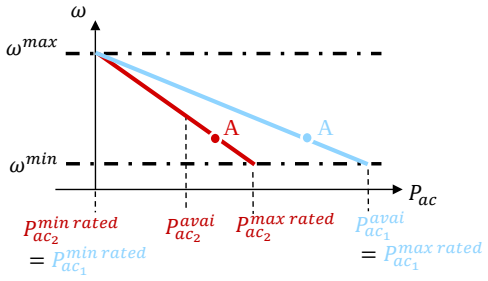

Figure 2: Possible scenario of the traditional P/ω droop when applied to inverter-based units interfacing intermittent energy sources.

In this scenario, the islanded microgrid could be perfectly stabilized at point A. This operating point, however, would result in the loss of Unit 2: since $P_{ac_2} > P_{ac_2}^{avai}$, the dc bus of Unit 2 would be progressively discharged and this unit would eventually shut down. Meanwhile, part of the available power of Unit 1 would remain unused. It is therefore clear that the traditional P/ω droop is not able to ensure the *no individual unit loss* feature. In addition, since $\omega > \omega^{min}$, no emergency load shedding would be activated to avoid the loss of Unit 2. This proves that the traditional P/ω droop loses the second essential feature (i.e., *the frequency limits signal the trespassing of active power limits*). It is therefore necessary to modify the traditional P/ω droop control, so that its resulting profile adapts to potential P_{ac}^{avai} variations.

3. Simulation Model

Fig. 3(a) represents the simulation model used in the analysis. It is a single-bus microgrid with two PV units, two lines and a switching resistive load connected to an UF relay, which sheds the last added load step if the frequency goes under ω^{min} for a predefined time threshold. This reduced islanded microgrid has been selected on purpose, to allow a clear visualization of the active power exchanges among the two PV units and the load.

Fig. 3(b) depicts a more detailed representation of the PV units model. The "Adaptive P/ω droop" block can be filled with the equations corresponding to any of the analyzed adaptive droop strategies. As mentioned, some of these strategies rely on a measurement of the dc bus voltage or on the available active power. The available active power (P_{ac}^{avai}) is actually equal to the available PV power (p_{pv}^{avai}) minus the losses occurring in the inverter and the dc/dc converter, which are here neglected. And the available PV power is typically obtained with measurement-based methods or estimation based methods [24] that, to a greater or a lesser extent, may be subject to errors. Consequently, in the simulation model, the adaptive droop strategies use a calculated available active power ($P_{ac}^{avai\,calc}$), which is equal to the true value of p_{pv}^{avai} plus a coefficient ϵ_{est} that models potential estimation errors.

Besides the inverter, it is essential to model the fact that the PV source may reach its maximum available power p_{pv}^{avai}, and that this upper limit can fluctuate because of irradiation (G) or temperature (T) changes. The upper part of Fig. 3(b) shows a complete model of a double-stage PV plant. Because the inverter is operated in grid-forming mode, the power produced by the PV array must be continuously adapted to the active power required by the islanded microgrid (i.e., P_{ac}). To achieve this, the block named "v_{dc} regulator" calculates the PV array power reference (p_{pv}^{ref}). More precisely, this block aims to regulate v_{dc}, by ensuring that the power going into the dc bus is equal to the power going out of it.

Then p_{pv}^{ref} is used by the block named "PV control", which is typically made up of two components [25]: first, a flexible power point tracking algorithm (FPPT) calculates the voltage that should be imposed on the PV array (v_{pv}) to obtain the power required by p_{pv}^{ref}; second, a regulator governing the dc/dc converter ensures that v_{pv} converges towards the value calculated by the FPPT. However, the "PV control" block and part of the dc side have been substituted by the simplified model shown in Fig. 3(b), since this allows a clearer evaluation of the adaptive droop strategies and of the impact of a p_{pv}^{avai} change on these strategies. An additional advantage of this simplification is that the resulting model is generic, and the obtained results are therefore extendable to other double-stage systems interfacing intermittent energy sources (e.g., type IV wind turbines).

Note that, since this article is focused on PV units and to ease the figures reading, the remaining sections assume that $P_{ac_i}^{min\,rated} = 0\,\forall i$.

4. Existing adaptive P/ω droop strategies analysis and comparison

4.1. Strategy α

In Strategy α [10], the traditional P/ω equation is complemented with a term proportional to $v_{dc}(t) - v_{dc}^{ref}$. Fig. 4(a) and (b) represent, respectively, the block diagram corresponding to this strategy and its resulting droop profiles. The added term impedes P_{ac} from exceeding P_{ac}^{avai} in the steady-state. Regarding the droop profiles, this term is equivalent to a vertical segment that intersects the traditional sloped segment at $P_{ac} = P_{ac}^{avai}$ and shifts horizontally as P_{ac}^{avai} varies.

Simulation Test 1 has been designed to illustrate the functioning of Strategy α and of the remaining strategies. The microgrid initially works at operating point A, in which the total active power consumed in the microgrid is smaller than the total available active power (i.e., $P_{cons} < P_{ac_1}^{avai} + P_{ac_2}^{avai}$). At $t = 0.5$ s,

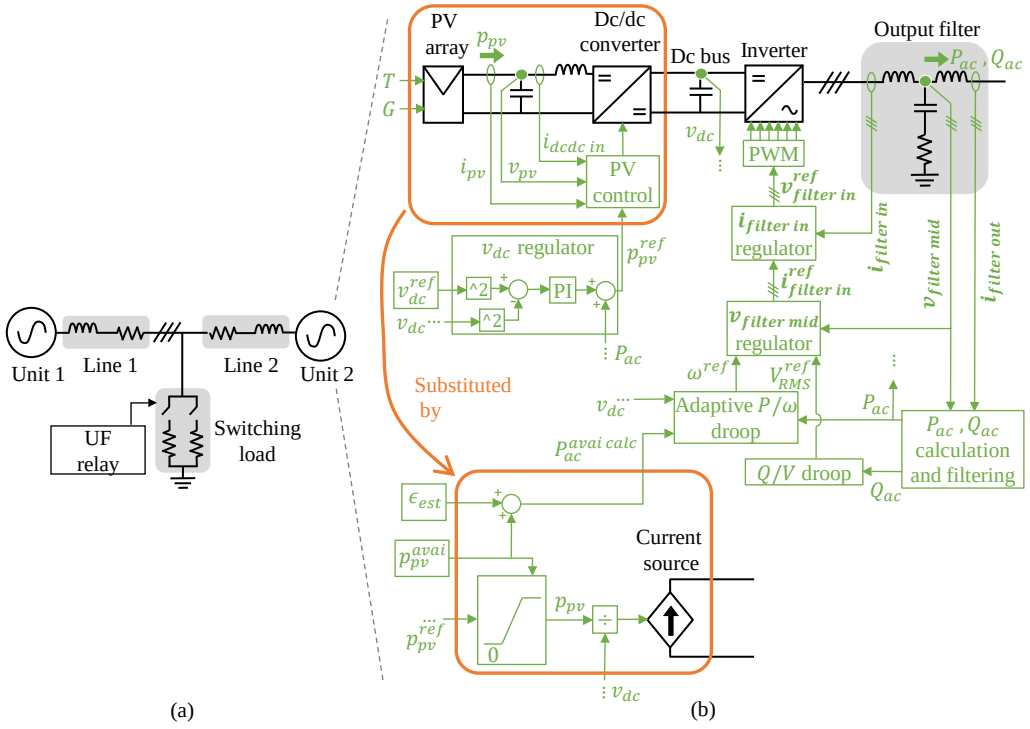

Figure 3: Simulation model: (a) islanded microgrid and (b) detailed view of the PV units composition and control scheme.

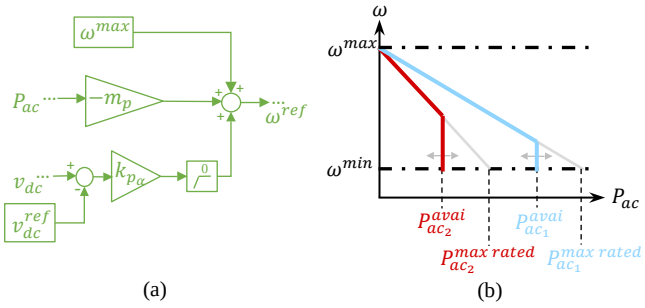

Figure 4: Strategy α, description. (a) Block diagram. (b) Droop profiles.

the load increases and the microgrid stabilizes at point B (still with $P_{cons} < P_{ac_1}^{avai} + P_{ac_2}^{avai}$). Finally, a second load increase happens at $t = 1.5$ s, after which $P_{cons} > P_{ac_1}^{avai} + P_{ac_2}^{avai}$. This should trigger the UF relay, which would shed the last added load and make the system return to point B.

Fig. 5(b)-(d) depict the temporal evolution of the main system variables. Fig. 5(a) depicts the droop profiles (solid lines) and the trajectories followed by the variables P_{ac} and ω during the test (arrowed lines). Note that, although a droop profile represents the set of operating points a PV unit can reach in steady state, the pair $[P_{ac}, \omega]$ may lay outside this set in transient operation. Note also that the depicted $[P_{ac}, \omega]$ trajectories are approximate, since they have been enlarged to improve the legibility of the image, reason why Fig. 5(a) is not at scale.

Initially, both PV units are working under their available active powers (point A). The load step of $t = 0.5$ s makes both P_{ac_1} and P_{ac_2} increase, which causes the drop of both v_{dc_1} and v_{dc_2}. This leads to the activation of the v_{dc} *regulators* and a consequent increase of p_{pv_1} and p_{pv_2}. In Unit 1, this increase is enough to contain the drop of v_{dc_1}, but in Unit 2 p_{pv_2} reaches $p_{pv_2}^{avai}$ and saturates. This is resolved by the added droop term: the bigger v_{dc_2} drop makes ω_2 decrease under ω_1. By means of the microgrid lines dynamics, this forces Unit 1 to further increase P_{ac_1}, allowing P_{ac_2} to decrease. The microgrid reaches operating point B at $t \approx 1$ s, in which:

- $P_{ac_2} = p_{pv_2} = P_{ac_2}^{avai}$. Consequently, v_{dc_2} stops dropping, but it stabilizes at a value smaller than $v_{dc_2}^{ref}$. More precisely, it stabilizes at a value such that $k_{p_{\alpha_2}} \times \left(v_{dc_2}^{ref} - v_{dc_2}\right) = \Delta\omega_{\alpha_2}^{B}$, where $\Delta\omega_{\alpha_2}^{B}$ is frequency drop needed for Unit 2 to enter the droop vertical segment and reach point B.
- $\omega_1 = \omega_2$, allowing the microgrid to reach a steady-state regime.
- $P_{ac_1} + P_{ac_2} = P_{cons}$.

After point B is reached, the load step of $t = 1.5$ s makes P_{ac_1} and P_{ac_2} increase, making the v_{dc} *regulators* actuate again: p_{pv_2} is already at its maximum, while p_{pv_1} increases and saturates as well. Consequently, both PV units experience a v_{dc} drop. By means of the added droop terms, ω_1 and ω_2 decrease and, eventually, go under ω^{min}. This activates the UF load shedding and brings the microgrid back to point B.

It is concluded that, by means of the added droop term, Strategy α preserves the essential droop features at high loadings (i.e., when P_{cons} approaches or goes beyond $\sum_{i=1}^{n} P_{ac_i}^{avai}$). In a certain unit, this new term impedes P_{ac} from stabilizing over P_{ac}^{avai} if there are other units in the microgrid which

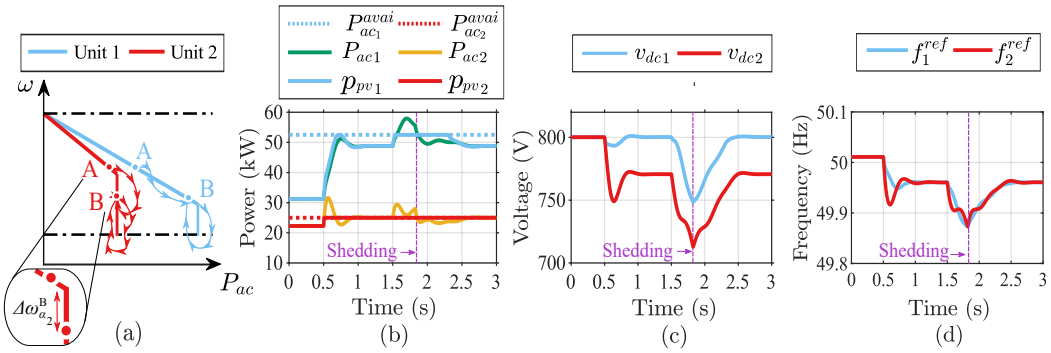

Figure 5: Strategy α, Test 1 results. (a) Droop profiles and approximate $[P_{ac}, \omega]$ trajectories. (b)-(d) Temporal evolution of variables of interest.

have not reached this limit. And, if $P_{cons} > \sum_{i=1}^{n} P_{ac_i}^{avai}$, this term makes the frequency drop under ω^{min}. Regarding operation at low loadings (i.e., when P_{cons} approaches or goes under $\sum_{i=1}^{n} P_{ac_i}^{min\,rated}$), it is not shown with Test 1, but the droop essential features are ensured by the sloped term of Strategy α, as they do in the traditional droop formulation of (1).

This sloped term also guarantees the accessory droop features at low loadings. Nevertheless, Test 1 shows that these are lost at high loadings:

- The PV units do not reach their available active powers at similar paces. At point A, for instance, Unit 2 operates close to $P_{ac_2}^{avai}$, while Unit 1 is far below $P_{ac_1}^{avai}$. Therefore, when the first load increase occurs, p_{pv_2} saturates before p_{pv_1}, and this results in a poorer transient performance of v_{dc_2} with respect to v_{dc_1}.
- Although the UF relay is correctly triggered, the activation of this relay is delayed. At point B, P_{cons} is close to $P_{ac_1}^{avai} + P_{ac_2}^{avai}$. Yet, the frequency of this operating point is well above ω^{min}. Consequently, when the second load increase occurs, the frequency must drop to ω^{min} for the UF relay to be triggered. And, the longer their triggering time, the more the dc bus voltages drop.

Another important downturn of Strategy α are the v_{dc} steady state errors (i.e., $v_{dc} < v_{dc}^{ref}$) experienced when the added droop segment is activated. Note that an excessive voltage reduction can disturb the functioning of the dc/dc converter or of the inverter. In contrast, other advantages of this strategy are that it does not comprise PI controllers that need to be reset and that it is not affected by $P_{ac}^{avai\,calc}$ overestimations, as it does not use this magnitude.

4.2. Strategy β

Strategy β [11] is a direct evolution of Strategy α, in which the proportional controller is substituted by a PI controller, to suppress the observed v_{dc} steady-state errors. Fig. 6(a) presents the block diagram of Strategy β and Fig. 6(b) the corresponding droop profiles (note that these are identical to those of Strategy α).

Note that there are two different PI controllers regulating $v_{dc}(t) - v_{dc}^{ref}$. On one hand, the is the v_{dc} *regulator* of Fig. 3

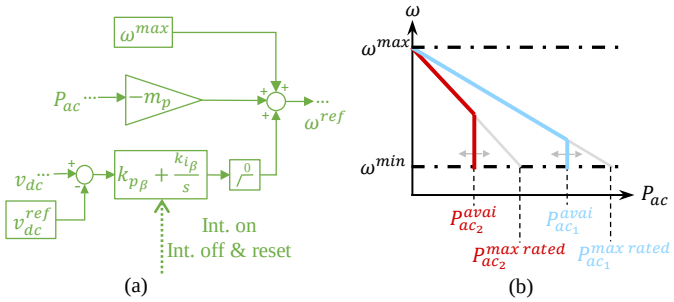

Figure 6: Strategy β, description. (a) Block diagram. (b) Droop profiles.

(PI_{dc}), which regulates v_{dc} when p_{pv}^{ref} is not saturated (its integral term is turned off by an anti-wind up system otherwise). On the other hand, there is the PI controller included in the droop scheme (PI_β), which should only regulate v_{dc} when p_{pv}^{ref} exceeds p_{pv}^{avai}. This is why PI_β includes a signal that turns its integrator on or off. In addition, when this integrator is deactivated, its output is reset to zero, allowing the PV units to leave the vertical segment of their droop profile once p_{pv}^{ref} becomes smaller than p_{pv}^{avai}, as it will be illustrated below.

Fig. 7 shows the results obtained by executing Test 1 on Strategy β. As in Strategy α, the load step of $t = 0.5$ s makes p_{pv_2} saturate and v_{dc_2} drop. In consequence, the new droop term decreases ω_2 under ω_1, which in turn forces P_{ac_1} to increase and allows P_{ac_2} to decrease. However, in this strategy, the new droop term not only makes P_{ac_2} decrease back to $P_{ac_2}^{avai}$ so that v_{dc_2} stops dropping, but it also forces v_{dc_2} to increase back to $v_{dc_2}^{ref}$. Eventually, the microgrid stabilizes at point B, in which:

- $P_{ac_2} = p_{pv_2} = P_{ac_2}^{avai}$ and $v_{dc_2} = v_{dc_2}^{ref}$. Note that it is the integrator of PI_β that creates the necessary frequency drop for Unit 2 to enter the droop vertical segment and reach point B.
- $\omega_1 = \omega_2$, allowing the microgrid to reach a steady-state regime.
- $P_{ac_1} + P_{ac_2} = P_{cons}$.

After this, the load increase of $t = 1.5$ s makes p_{pv_1} saturate as well, which leads to an unceasing drop of v_{dc_1} and v_{dc_2}, causing the load shedding activation. This allows the dc bus voltages to

recover and both p_{pv_1} and p_{pv_2} desaturate at $t \approx 2.3$ s. Consequently, in both units, the PI_β integrator is turned off and its output is reset. For Unit 2, this reset is not essential in the depicted scenario, since p_{pv_2} resaturates soon after and the integrator is turned on again. But the reset allows Unit 1 to leave the vertical segment of its droop profile and go back to operating point B. Nevertheless, the downturn of the resetting procedure is that it may provoke considerable ω steps, leading to unwanted P_{ac} and v_{dc} fluctuations, as seen in Fig. 7.

Note that [12] proposes a different management of the alternations between PI_{dc} and PI_β, that does not require the reset of PI_β. However, it requires a different v_{dc} *regulator*, which includes a switch signal that may also lead to unwanted oscillations.

Except for the absence of v_{dc} steady-state errors and the need for a reset of PI_β, the rest of the conclusions derived for Strategy α (e.g., loss of the accessory droop features at high loadings) also apply to Strategy β.

4.3. Strategy γ

As for the previous strategies, Strategy γ [13] relies on the creation of a vertical droop profile (Fig. 8(b)). However, in this case the vertical segment is achieved with a PI controller that is activated when $P_{ac} - P_{ac}^{avai\,calc} > 0$, as shown on Fig. 8(a).

For the sake of brevity, the results obtained by executing Test 1 on Strategy γ are not included in this paper. However, the droop profiles resulting from this strategy have identical shapes to those of Strategy α and of Strategy β. In can be therefore concluded that Strategy γ also preserves the essential droop features both at high and at low loadings, but the accessory features are only preserved at low loadings.

Additionally, the control scheme of Fig. 8(a) allows to deduce that, with Strategy γ, the dc bus voltage may be subject to steady-state errors when the added droop term is activated. When a load step makes P_{ac} increase over $P_{ac}^{avai\,calc}$, PI_γ is activated and makes P_{ac} decrease back to $P_{ac}^{avai\,calc}$. Consequently, v_{dc} stops dropping, but no control mechanism forces it to increase back to v_{dc}^{ref}. The v_{dc} steady-state errors are common to Strategy α, but in this strategy the magnitude of the error depends on the selected k_{p_α}, while in Strategy γ it is completely ungoverned. On another note, it is also deduced from Fig. 8(a) that PI_γ does not require to be reset for a unit to leave the vertical segment of its droop profile and go back to the sloped segment. When P_{ac} decreases below $P_{ac}^{avai\,calc}$, PI_γ increases its output. As it is not necessary to turn off its integrator (since no other PI controller regulates P_{ac}), the output of PI_γ eventually saturates at 0.

Finally, Strategy γ presents a major drawback, since it relies on an estimation of P_{ac}^{avai} that may be erroneous. The most problematic scenario is the case of an overestimation (i.e., $P_{ac}^{avai\,calc} > P_{ac}^{avai}$). To illustrate this, Strategy γ is subjected to a new simulation test (Test 2), in which Unit 2 experiences an overestimation error. Fig. 9 displays the results of this test (note that the vertical segment of Unit 2 is shifted from the true value of $P_{ac_2}^{avai}$).

Initially, the microgrid operates at point A and, at $t = 0.25$ s, it experiences a load step that makes it shift to point B. Since $P_{ac_1} < P_{ac_1}^{avai\,calc}$ and $P_{ac_2} < P_{ac_2}^{avai\,calc}$, the ac side of the microgrid stabilizes with $\omega > \omega^{min}$, and no load shedding occurs. However, as $P_{ac_2}^{avai\,calc}$ is erroneous, P_{ac_2} is actually greater than $P_{ac_2}^{avai}$, causing the progressive drop of v_{dc_2} and the eventual disconnection of Unit 2. This could be avoided with a mechanism that, at operating point B, transferred part of the load fed by Unit 2 to Unit 1. However, Strategy γ does not provide such a mechanism.

Note that [16] proposes a variant of Strategy γ in which the PI controller regulates the difference between the available apparent power and the measured apparent power ($S_{ac}^{avai\,calc} - S_{ac}$). However, as in Strategy γ, the proportional power sharing is lost at high loadings. Furthermore, [16] does not address the potential problems caused by a wrong $S_{ac}^{avai\,calc}$ estimation nor the dc bus voltage regulation issues.

4.4. Strategy δ

The first three strategies add a vertical segment to the traditional P/ω droop profile. However, Strategy δ [14, 15, 17] is based on a different principle: a varying droop slope $\hat{m}_p$, that makes the droop profile follow the point $[P_{ac}^{avai\,calc}(t), \omega^{min}]$. Fig. 11(a) depicts the control scheme of Strategy δ and Fig. 11(b) its associated droop profiles.

The working principle and equations of Strategy δ are nearly equal to those of the traditional P/ω droop. The only difference is the adaptive slope, that allows the sloped droop profile to go through both point $[P_{ac}^{min\,rated} = 0, \omega^{max}]$ (fixed) and point $[P_{ac}^{avai\,calc}(t), \omega^{min}]$ (moving). In consequence, Strategy δ preserves all the essential and accessory droop features, both at high and at low loadings.

It should also be noted that, except in the case of positive $P_{ac}^{avai\,calc}$ errors, Strategy δ allows an adequate regulation of the dc bus voltage at all steady state operating points. Whenever the microgrid is working under its full load (i.e., $P_{cons} < P_{ac_1}^{avai} + P_{ac_2}^{avai}$), each of the PV units works under its full load too (i.e., $P_{ac_i} < P_{ac_i}^{avai}$, $i = 1, 2$). Consequently, their v_{dc} *regulators* do not saturate and can regulate v_{dc} to v_{dc}^{ref}. When $P_{cons} > P_{ac_1}^{avai} + P_{ac_2}^{avai}$, all the PV units saturate and their dc bus voltages drop, but in this case the frequency is reduced under ω^{min} and the UF load shedding is triggered.

Despite all these merits, Strategy δ has the same major drawback as Strategy γ: it relies on $P_{ac}^{avai\,calc}$, which might be erroneous and provoke the loss of a PV unit.

Finally, another considerable drawback of Strategy δ is that $\hat{m}_p$ has a direct influence on stability. Increasing this slope causes an ample migration of the poles associated with the P/ω droop control towards the imaginary axis, which decreases the system stability margin. This is demonstrated in the small-signal stability analyses of [23] and [26], and illustrated by executing a new test (Test 3, Fig. 10). The microgrid, initially operating at point A, experiences a load step at $t = 0.5$ s that makes it shift to point B. It is observed that the microgrid presents an adequate dynamic response after this disturbance. Then, at $t = 1.5$ s, Unit 2 experiences an irradiation decrease (i.e., $p_{pv_2}^{avai}$ is reduced), after which point C is reached. Finally, at $t = 2.5$ s, a new load step occurs (of the same magnitude than the first

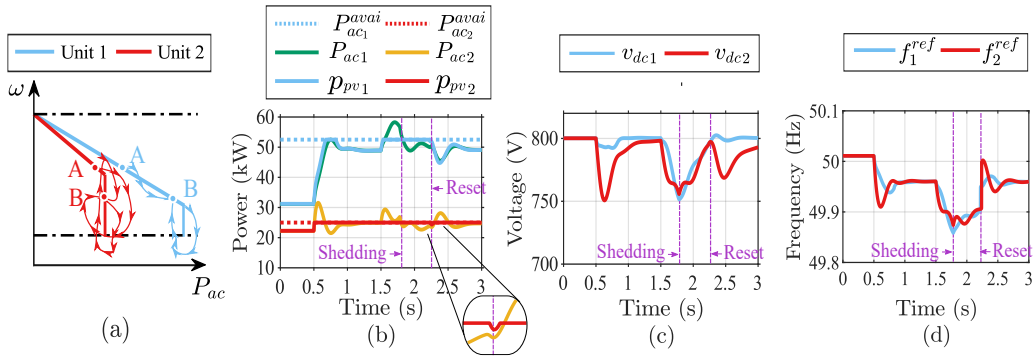

Figure 7: Strategy β, Test 1 results. (a) Droop profiles and approximate $[P_{ac}, \omega]$ trajectories. (b)-(d) Temporal evolution of variables of interest.

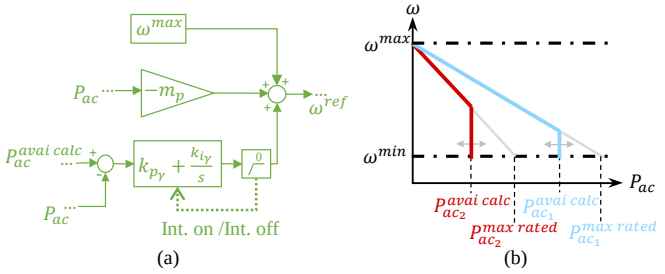

Figure 8: Strategy γ, description. (a) Block diagram. (b) Droop profiles.

load step). It is observed that the microgrid presents a much less damped dynamic behavior after the second load step, once $p_{pv_2}^{avai}$ has been reduced.

As proposed by [14], this major pole displacement can be countered with compensators such as virtual impedances or power system stabilizers. However, in microgrids with multiple PV units, it would challenging for these compensators to work without communication links, since the poles to be redressed would be affected by the droop slopes of PV units placed at different locations. Another option, proposed by [17], is to mitigate the consequences of the pole displacement by configuring each PV unit with a saturation function that limits the value of the adaptive droop slope. Additionally, the droop scheme is complemented by a vertical segment, such as the one proposed in Strategy β, that is activated whenever the upper limit of $\hat{m}_p$ is reached.

5. Conclusions

Islanded operation is a key tool to improve the reliability and operational resilience of distribution grids, for instance in the case of extreme weather events that make the main grid unavailable. To enable an islanded operation with minimal hardware changes, it is convenient to operate already installed PV units in droop-controlled grid-forming mode. This paper has analyzed the main adaptive strategies that allow to implement the P/ω droop principle in double-stage units interfacing intermittent energy sources. The advantages and unwanted behaviors of each strategy have been illustrated by means of a thorough simulation-based evaluation whose results are summarized in Table 1. Additionally, such evaluation allows to compose the following set of guidelines for the design of novel improved adaptive P/ω droop strategies:

- Most of the analyzed strategies preserve a fixed droop slope starting at $[P_{ac}^{min\ rated} = 0, \omega^{max}]$ and crossing a vertical segment placed at P_{ac}^{avai} or $P_{ac}^{avai\ calc}$. This allows to preserve the essential droop features, but the accessory features are preserved only at low loadings.

- To preserve the accessory features at high loadings (which is more adequate, in general, for an emergency islanding scenario with energy scarcity), the slope segment should end at the point $[P_{ac}^{avai\ calc}(t), \omega^{min}]$.

- Therefore, to preserve all features both at high and at low loadings, an adaptive droop slope going from $[P_{ac}^{min\ rated} = 0, \omega^{max}]$ to $[P_{ac}^{avai\ calc}(t), \omega^{min}]$ should be used. But the increase of this slope causes an ample migration of critical poles towards the imaginary axis.

- There are three options to create a vertical droop segment (a proportional controller on $v_{dc}(t) - v_{dc}^{ref}$, a PI controller on $v_{dc}(t) - v_{dc}^{ref}$ and a PI controller on $P_{ac}^{avai\ calc}(t) - P_{ac}(t)$). Each leads to a different side effect regarding the regulation of v_{dc}.

- The strategies relying on $P_{ac}^{avai\ calc}$ have a considerable drawback since this magnitude may be obtained with methods prone to errors. More precisely, an overestimation of $P_{ac}^{avai\ calc}$ can provoke the loss of a PV unit. In this sense, these strategies are outperformed by the those using a v_{dc} measurement, which is a reliable indicator of a PV unit loading.

Finally, it should be noted that, although the simulated microgrid presents only two PV units for illustrative reasons, the analyzed strategies are expandable to any number of units. Furthermore, it is possible to combine units controlled with these adaptive P/ω droop strategies and dispatchable generators controlled with the traditional droop control (to extend islanded operation to hours without solar resource, for instance).

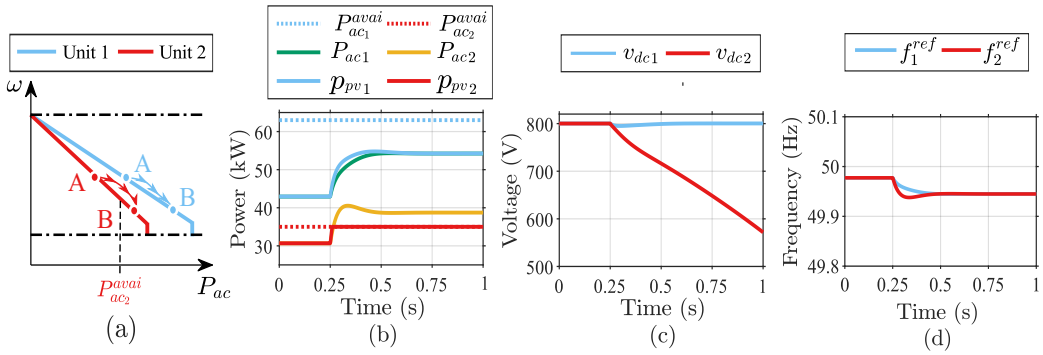

Figure 9: Strategy γ, Test 2 results. (a) Droop profiles and approximate $[P_{ac}, \omega]$ trajectories. (b)-(d) Temporal evolution of variables of interest.

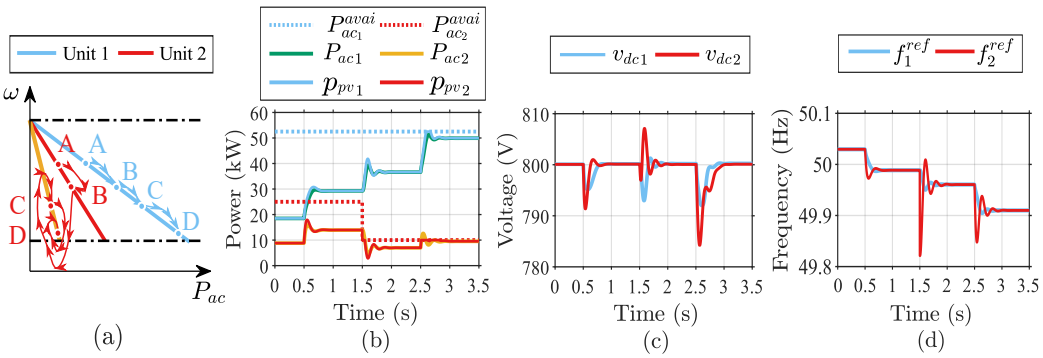

Figure 10: Strategy δ, Test 3 results. (a) Droop profiles and approximate $[P_{ac}, \omega]$ trajectories. (b)-(d) Temporal evolution of variables of interest.

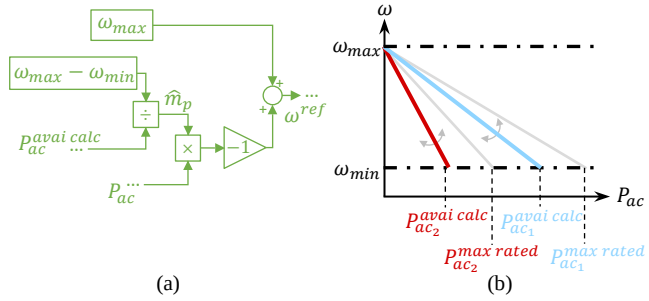

Figure 11: Strategy δ, description. (a) Block diagram. (b) Droop profiles.

Acknowledgments

This work has been funded under the scope of the NTU-CNRS "Excellence Science" joint research program.

References

[1] IEA, Climate Resilience, Technical Report, 2021. URL: `https://www.iea.org/reports/climate-resilience`.

[2] R. Bayani, S. D. Manshadi, Resilient expansion planning of electricity grid under prolonged wildfire risk, IEEE Transactions on Smart Grid 14 (2023) 3719–3731.

[3] How climate-related weather conditions disrupt power plants in Indonesia and affect people | UNDRR PreventionWeb, 2020. URL: `https://www.preventionweb.net/news/how-climate-related-weather-conditions-disrupt-power-plants-indonesia-and-affect-people`.

[4] CIRED Working Group 2018-03, Technical requirements for the operation of microgrids in both interconnected and islanded modes, Technical Report, 2021. URL: `http://www.cired.net/cired-working-groups`.

[5] M. Mahzarnia, M. P. Moghaddam, P. T. Baboli, P. Siano, A review of the measures to enhance power systems resilience, IEEE Systems Journal 14 (2020) 4059–4070.

[6] What is the Distributed ReStart project? | National Grid ESO, 2023. URL: `https://www.nationalgrideso.com/future-energy/projects`.

[7] IEA, Solar PV, Technical Report, 2021. URL: `https://www.iea.org/reports/solar-pv`.

[8] H. Han, X. Hou, J. Yang, J. Wu, M. Su, J. M. Guerrero, Review of power sharing control strategies for islanding operation of ac microgrids, IEEE Transactions on Smart Grid 7 (2016) 200–215.

[9] D. E. Olivares, A. Mehrizi-Sani, A. H. Etemadi, C. A. Cañizares, R. Iravani, M. Kazerani, A. H. Hajimiragha, O. Gomis-Bellmunt, M. Saeedifard, R. Palma-Behnke, G. A. Jiménez-Estévez, N. D. Hatziargyriou, Trends in microgrid control, IEEE Transactions on Smart Grid 5 (2014) 1905–1919.

[10] H. Liu, Y. Yang, X. Wang, P. C. Loh, F. Blaabjerg, W. Wang, D. Xu, An enhanced dual droop control scheme for resilient active power sharing among paralleled two-stage converters, IEEE Transactions on Power Electronics 32 (2017) 6091–6104.

[11] H. Mahmood, J. Jiang, Decentralized power management of multiple PV, battery, and droop units in an islanded microgrid, IEEE Transactions on Smart Grid 10 (2019) 1898–1906.

[12] B. Pawar, E. I. Batzelis, S. Chakrabarti, B. C. Pal, Grid-forming control for solar PV systems with power reserves, IEEE Transactions on Sustainable Energy 12 (2021) 1947–1959.

[13] Z. Chen, R. H. Lasseter, T. M. Jahns, Active power reserve control for grid-forming PV sources in microgrids using model-based maximum power point estimation, in: 2019 IEEE Energy Conversion Congress and Exposition (ECCE), 2019, pp. 41–48.

[14] Z. Li, K. W. Chan, J. Hu, J. M. Guerrero, Adaptive droop control using adaptive virtual impedance for microgrids with variable PV outputs and load demands, IEEE Transactions on Industrial Electronics 68 (2021)

9630–9640.

[15] N. L. Díaz, J. C. Vasquez, J. M. Guerrero, A communication-less distributed control architecture for islanded microgrids with renewable generation and storage, IEEE Transactions on Power Electronics 33 (2018) 1922–1939.

[16] B. She, F. Li, H. Cui, J. Wang, L. Min, O. Oboreh-Snapps, R. Bo, Decentralized and coordinated V-f control for islanded microgrids considering DER inadequacy and demand control, IEEE Transactions on Energy Conversion 38 (2023) 1868–1880.

[17] M. Su, K. Zhang, Y. Sun, H. Han, G. Shi, S. Fu, Coordinated control for PV-ESS islanded microgrid without communication, International Journal of Electrical Power & Energy Systems 136 (2022) 107699.

[18] F. Kelada, J. Buire, N. Hadjsaid, Comparative study of decentralized grid-forming converter control for inverter based microgrids, in: 2023 IEEE Power & Energy Society General Meeting (PESGM23), 2023.

[19] R. Rosso, X. Wang, M. Liserre, X. Lu, S. Engelken, Grid-forming converters: Control approaches, grid-synchronization, and future trends—a review, IEEE Open Journal of Industry Applications 2 (2021) 93–109.

[20] A. K. Sahoo, K. Mahmud, M. Crittenden, J. Ravishankar, S. Padmanaban, F. Blaabjerg, Communication-less primary and secondary control in inverter-interfaced ac microgrid: An overview, IEEE Journal of Emerging and Selected Topics in Power Electronics (2020) 1–1.

[21] Y. W. Li, C.-N. Kao, An accurate power control strategy for power-electronics-interfaced distributed generation units operating in a low-voltage multibus microgrid, IEEE Transactions on Power Electronics 24 (2009) 2977–2988.

[22] J. He, Y. W. Li, J. M. Guerrero, F. Blaabjerg, J. C. Vasquez, An islanding microgrid power sharing approach using enhanced virtual impedance control scheme, IEEE Transactions on Power Electronics 28 (2013) 5272–5282.

[23] N. Pogaku, M. Prodanovic, T. C. Green, Modeling, analysis and testing of autonomous operation of an inverter-based microgrid, IEEE Transactions on Power Electronics 22 (2007) 613–625.

[24] Q. Peng, A. Sangwongwanich, Y. Yang, F. Blaabjerg, Grid-friendly power control for smart photovoltaic systems, Solar Energy (2020).

[25] H. D. Tafti, G. Konstantinou, C. D. Townsend, G. G. Farivar, A. Sangwongwanich, Y. Yang, J. Pou, F. Blaabjerg, Extended functionalities of photovoltaic systems with flexible power point tracking: Recent advances, IEEE Transactions on Power Electronics 35 (2020) 9342–9356.

[26] A. Firdaus, S. Mishra, Mitigation of power and frequency instability to improve load sharing among distributed inverters in microgrid systems, IEEE Systems Journal 14 (2020) 1024–1033.

Table 1: Evaluation summary for Strategies α, β, γ, and δ.

Feature	Achieved for α?	Achieved for β?	Achieved for γ?	Achieved for δ?
Frequency limits signal the trespassing of active power limits	Yes	Yes	Yes	Yes
No individual unit loss	Yes	Yes	Yes	Yes
Fast reactivity of frequency-based protections	Only at low loadings	Only at low loadings	Only at low loadings	Yes
Reach of active power limits at equal pace	Only at low loadings	Only at low loadings	Only at low loadings	Yes
No PIs to reset	Yes	No (PIs to reset that may cause unwanted fluctuations)	Yes	Yes
Correct v_{dc} regulation	No, steady state error in vertical droop segment	Yes	No, ungoverned steady state error in vertical droop segment	Yes
Robustness against $P_{ac}^{pwat\,calc}$ overestimation	Yes (does not use $P_{ac}^{pwat\,calc}$)	Yes (does not use $P_{ac}^{pwat\,calc}$)	No, potential PV unit loss	No, potential PV unit loss
(Additional advantages/disadvantages)				$\hat{m}_p$ variations cause critical poles displacements